A liquid-He cryostat for structural and thermal disorder studies by X-ray absorption

F. Bouamrane, M. Ribbens, E. Fonda, C. Adjouri and A. Traverse*

Laboratoire pour l'Utilisation de Rayonnement Electromagnétique (LURE), BP 34, 91898 Orsay, France. E-mail: agnes.traverse@lure.u-psud.fr

A new device operating from 4.2 to 300 K is now installed on the hard X-ray station of the DCI ring in LURE in order to measure absorption coefficients. This liquid-He bath device has three optical windows. One allows the incident beam to impinge on the sample, one located at 180° with respect to the sample allows transmitted beams to be detected, and another located at 90° is used to detect emitted photons. Total electron yield detection mode is also possible thanks to a specific sample holder equipped with an electrode that collects the charges created by the emitted electrons in the He gas brought from the He bath around the sample. The performance of the cryostat is described by measurements of the absorption coefficients *versus* the temperature for Cu and Co foils. For comparison, the absorption coefficient is also measured for Cu clusters. As expected from dimension effects, the Debye temperature obtained for the clusters is lower than that of bulk Cu.

Keywords: X-ray absorption spectroscopy; solid clusters; X-ray and γ-spectroscopy.

1. Introduction

Third-generation synchrotrons now provide photon beams with high brilliance and very good position stability (Level *et al.*, 2002). Among the techniques available around a synchrotron, X-ray absorption spectroscopy (XAS) is a powerful and well established tool that allows experimentalists to obtain information on the local structure of a given type of atom, thanks to its chemical selectivity. XAS is widely used in solid-state physics, catalysis, coordination chemistry and biology; a great flexibility of the sample environment and in the available detection modes is thus a necessity.

Extended X-ray absorption fine structure (EXAFS) provides unique information since it measures the interatomic distance distribution for each coordination shell of the absorber atom. The analysis of the dependence of the mean square root displacement (MSRD) *versus* the temperature (T) in the range from ambient down to 4 K permits the thermal and static contributions to the distribution of interatomic distances to be separated and the model potentials on the measured distributions to be tested (Dalba & Fornasini, 1997).

In the single-scattering approach, the expression of the EXAFS oscillations is given by

$$\chi(k) = \sum_i (N_i/kr_i^2) f_i(k,p) \sin\left[2kr_i + \varphi_i(k)\right] \times \exp\left(-2k^2\sigma_i^2\right) \exp\left[-2r_i/\lambda_i(k)\right],$$

where k is the wavevector and f_i is the probability of scattering at 180° by the atom i located on shell i at distance r_i from the absorber. There are N_i neighbours in this shell. φ_i is the phase shift due to the nature of both the absorbing and scattering atom. The first correction term contains the Debye–Waller factor σ_i, which is a measure of the structural and thermal disorders. The second correction term contains the mean free path of the photoelectrons, λ_i.

In this formula the disorder is accounted for by the term σ that can be written as $\sigma = \sigma^2_{\rm struc} + \sigma^2(T)$, where $\sigma^2_{\rm struc}$ is the structural term. The temperature-dependent term, $\sigma^2(T)$, is often described by the Debye correlated model (Sevillano & Meuth, 1979; Dalba & Fornasini, 1997; Bohmer & Rabe, 1979),

$$\sigma_j^2(\omega_{\rm D}, T) = \left(3\hbar/2\omega_{\rm D}^3\mu\right) \int_0^{\omega_{\rm D}} {\rm d}\omega\, \omega \coth(\hbar\omega/2kT) \times \left[1 - \sin\left(\omega q_{\rm D} R_j^0/\omega_{\rm D}\right)/\left(\omega q_{\rm D} R_j^0/\omega_{\rm D}\right)\right]$$

where T is the temperature, R_j is the distance between the atoms, μ is the reduced mass, $\omega_{\rm D}$ is the Debye cut-off frequency, and the Debye temperature is $\theta_{\rm D} = \hbar\omega_{\rm D}/k_{\rm B}$. In the high-temperature range, $\sigma^2(T)$ is proportional to $T/\omega_{\rm D}^2$.

In the case of measurements performed close to the Debye temperature, anharmonic effects have to be considered and an analysis in terms of cumulants has to be performed (Dalba *et al.*, 1995). The cumulants are defined in the following way: $C_1(T) = \langle r\rangle$; $C_2(T) = \langle (r - \langle r\rangle)^2\rangle = \sigma_j^2$; $C_3(T) = \langle (r - \langle r\rangle)^3\rangle$. The third cumulant has to be introduced in the phase shift that becomes $\varphi'(k) = \varphi(k) - 4/3C_3k^3$ and C_3 varies with T^2.

Enhancement of anharmonic effects is expected in low-dimension systems, *i.e.* thin films (Kiguchi *et al.*, 1997), clusters (Pinto *et al.*, 1995) and at the surface of bulk materials (Balerna & Mobilio, 1986). The result is a lowering of the Debye temperature as compared with the bulk temperature. In Ni and Cu films (Kiguchi *et al.*, 2000), angular- and temperature-dependence of EXAFS lead to Debye temperatures of 83% and 91% of the bulk values, respectively. In ultrafine-grained Ni the decrease is even larger and the Debye temperature is 78% of the bulk value (Zhang *et al.*, 1998). Calculations also predict such behaviour in Co clusters (Hou *et al.*, 2000).

Samples of thin films, deposited clusters and embedded clusters usually contain a small quantity of absorbing atoms and are supported on thick substrates. This makes measurements in the transmission mode almost impossible. Techniques based on the detection of emitted electrons (TEY) or of fluorescence radiation are used instead. This is the reason why we developed a new device operating from 4.2 to 300 K where the three detection modes are possible and that is adapted to the constraints of beamline operations. This liquid-He bath cryostat was installed and tested on the D42 station of the DCI ring in LURE.

To illustrate the performances of the cryostat, we have studied the temperature dependence of the XAS pair distribution function on Co and Cu foils and on Cu clusters embedded in a Si_3N_4 matrix. Measurements have been made in transmission and TEY modes.

The paper is organized as follows. In the first section, the cryostat is described together with the sample holders designed for each detection mode. Some characteristics of the device are given together with indications on the quality of the signal in terms of electronic noise. In the second section, experimental data and their treatment are presented. In the final section, results are briefly discussed and compared with literature data.

2. Description of the cryostat

Low-temperature devices were already available at LURE. A 4–300 K cryostat for transmission was used for lattice dynamics studies (Fornasini, 2001, and references therein). A liquid-nitrogen-temperature apparatus, built to operate in the total electron yield mode (Mimault *et al.*, 1994), was used for structural characterization of epitaxically grown thin films (Andrieu *et al.*, 1996) or of clusters embedded in matrices (Zanghi *et al.*, 2000). Some of the trends

adopted in these devices were kept for the He bath cryostat described below.

2.1. Cooling device

The cooling device is a standard Air Liquide system made of a liquid-He reservoir (6 litres) enclosed in an annular liquid-nitrogen-cooled cryo-shield. The apparatus is diagrammatically shown in Fig. 1. The sample space with a volume of 28 cm^3, located at the bottom of the cryostat, is equipped with three optical windows (diameter 16 mm) made of kapton (thickness 25 μm). One window allows the incident photon beam to enter the chamber and to impinge on the sample. A second window, located at 180° with respect to the sample, allows transmitted photons to be detected in a classical gas-filled detector (Fig. 2). A third window located at 90° allows the detection of emitted photons thanks to a fluorescence detector. Actually, owing to the choice of a convection cryostat, each optical aperture is made by a couple of windows (25 μm of kapton each) since a primary vacuum separates the cryostat from the outside environment. The thickness of the kapton windows imposes a lower limit to the accessible energy range of X-ray photons: at 2 keV the transmission through the couple of entrance windows is 14% and that through the four windows is only 0.2%. At 2.75 keV transmission through the four windows is 14% and measurements in the transmission mode become feasible, but not optimal. Measurements between 2 and 2.75 keV could be envisaged in the TEY mode only, since the detection is made on the electron current inside the chamber.

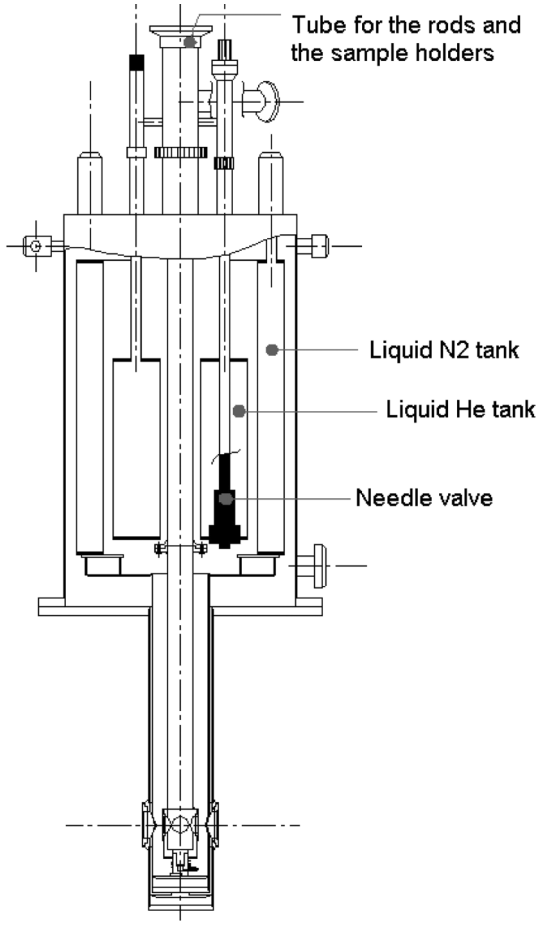

Figure 1
Simplified cross-sectional view of the cryostat.

To cool the sample, liquid He is drawn from the liquid-He reservoir through a capillary tube in the chamber. The flow is regulated by a needle valve (Fig. 1).

Once the liquid-N_2 reservoir has been filled and a temperature of about 200 K has been reached at the sample level, the lowest temperature of 4.2 K is quickly reached within 15 min after the end of the liquid-He transfer. The He reservoir lifetime is variable depending on the He flow. It is about 44 h when keeping the temperature at 20 K with a minimal He flux. The lifetime decreases to 8–9 h when working at 4.5 K and it is usually 24 h when operating at different temperatures between 10 and 200 K. Refilling the He reservoir takes 30 min at most, but during this time the temperature is not controlled and beamline operations must be stopped. Absolute thermal stability is about ±0.01 K in the range 4–100 K as measured by the thermocouple on the sample holder. Sample thermal stability is attained in about 1 h after the cryostat has reached the desired temperature. If the cryostat temperature is higher than 100 K, the sample needs more time to reach the same stability, since the He flow is reduced.

2.2. Rods and sample holders

The sample holder is fixed onto a rod that may be inserted and removed from the sample chamber through a central tube while the cryostat is maintained at low temperature, thus allowing a fast sample change (Fig. 1).

The rod can be height-adjusted and rotated. The range of vertical motion is 25 mm allowing three to four samples with dimensions as large as 4 mm × 14 mm to be successively measured in transmission or fluorescence mode, while keeping them at the same temperature (Fig. 2). The rotation is available on ±180°. This allows the experimentalist to benefit from the polarized character of the photon by varying the angle between the incident beam and the sample surface. For fluorescence, this rotation is necessary to adjust the sample surface in front of the detector. Vertical and rotational motions are computer-controlled from outside of the experimental hutch.

Fine temperature control is achieved by equilibrating the cooling He flow with a heating resistance. The heater is operated by a controller that simultaneously checks the thermocouple mounted in

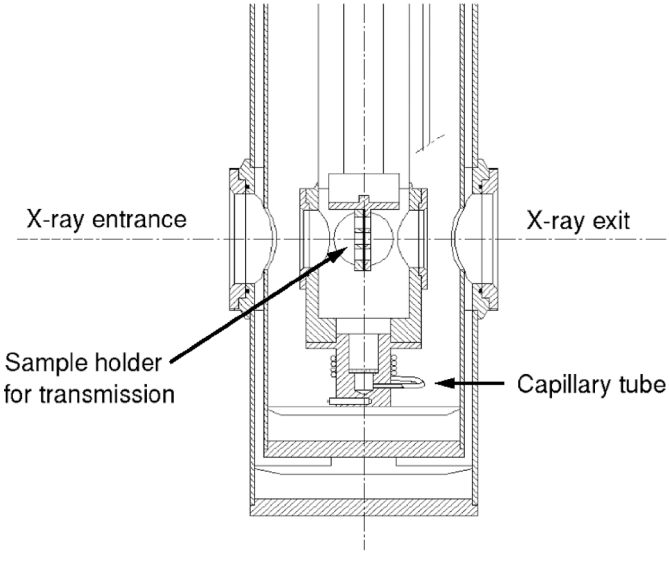

Figure 2
Sample space at the bottom of the cryostat with the optical windows and the sample holder for transmission.

the sample chamber. Another sensor, located on the rod near the sample holder, is used for measuring the sample temperature.

Several sample holders are available. Those for transmission and fluorescence are Cu or Al frames where the samples can be glued or clamped. The sample holder for TEY is a Cu square with a platform where the sample can be glued with electrical conductive silver paint. The charge collector, made of stainless steel, is fixed on the vertical part and is electrically insulated from the rod. The inclination angle of the sample support relative to the horizontal direction of the incoming X-ray beam is 30°. The signal is collected by a low-noise cable and measured with an ampere meter. The dark current is 0.1 (1) pA.

2.3. Absorption coefficient

In transmission mode the absorption coefficient is $\mu = \log (I_0/I_1)$ where I_0 and I_1 are the currents measured in ionization chambers located before and after the sample, respectively. In the cases of the fluorescence (Lee *et al.*, 1999) and TEY (Proux *et al.*, 2001) modes, and if the samples are appropriately prepared, the absorption coefficient is $\mu = I_1/I_0$ where I_0 has the same meaning as before. I_1 is proportional to the number of emitted photons in the fluorescence mode whereas in the TEY mode it is proportional to the number of emitted electrons. For TEY the exchange He gas, present around the sample, is used as a signal amplifier, so that this detector works on the same principle as those previously developed at LURE either for room-temperature measurements (Tourillon *et al.*, 1987) or for measurements at 80 K (Mimault *et al.*, 1994).

Since an electronic signal transported from the sample to the ampere meter is used in TEY, particular attention has to be paid to the quality of the signal. Typical values of $\Delta\mu/\mu$ were below 10^{-3} in all the measurements irrespective of the sample temperature.

3. Experimental data and treatment

Several absorption coefficients were measured at different temperatures ranging from 20 to 300 K. Two of the samples were foils. In the case of the Cu foil, 4 μm thick, the measurement was performed at the *K* edge (8979 eV) in the transmission mode. For the Co foil (*K* edge at 7709 eV) and Cu clusters embedded in a Si_3N_4 matrix (*K* edge at 8979 eV) the total conversion electron yield detection was selected. The preparation technique for the sample containing Cu clusters has already been described (Zanghi *et al.*, 2001). We recall that Si_3N_4 amorphous layers, 830 Å thick, were prepared using the dual-ion-beam sputtering technique. Argon ions (energy = 1.2 keV, flux = 80 mA) sputtered a Si_3N_4 target. The target and the sample holder (heated to 673 K), facing each other, were tilted 45° away from the incident beam. For good stoichiometry, samples were irradiated during the Si deposition with a N beam (energy = 50 eV, flux = 40 mA). Implantations were carried out at 300 K on the Irma implanter (Chaumont *et al.*, 1981) with 6×10^{16} Cu cm^{-2} at 150 keV. This incident energy was chosen so that the Cu ions stop in the layer. Implantation was followed by an annealing at 1073 K for 1 h under vacuum, a temperature that allows an increase of the cluster size (Zanghi *et al.*, 2000).

The EXAFS oscillations were extracted using a conventional signal treatment where a linear background calculated by extrapolating the pre-edge signal is first subtracted. Then the atomic absorption is subtracted assuming that it is well reproduced by a polynomial of degree 5. The signal is finally normalized (Michalowicz, 1991). The whole data set for one sample, *i.e.* the absorption coefficients taken at six or seven different temperatures, was treated in exactly the same way to extract the oscillations. Since the low-temperature measurements of the absorption coefficients in well ordered materials result in a noticeable enhancement of the signal coming from the upper neighbouring shells around the absorbing atom, the fit has been performed in *r*-space over the contributions in the range 1 Å $\leq r \leq$ 6 Å. Data analysis was performed using the *IFEFFIT* software and error bars are those provided by this code (Newville, 2001). Theoretical scattering phase shifts and amplitudes were calculated using the *FEFF7* code (Mustre de Leon *et al.*, 1991).

Table 1
Debye temperature, σ^2 at 300 K, and S_0^2 deduced from the fit.

Error bars are quoted in parentheses. An asterisk indicates that no error bar was given in the reference.

Θ_D (K)	σ^2 (10^{-3} Å^2)	S_0^2
439 (16)†		
385 (*)‡	5.2 (3)†	0.75 (2)†
445 (*)§	5.1 (*)¶	
395 (*)††		

† Present work. ‡ Ashcroft & Mermin (1988). § Kittel (1966). ¶ Jacobs & Egry (1999). †† Hou *et al.* (2000).

4. Results and discussion

Extended X-ray absorption fine structure (EXAFS) oscillations extracted from the absorption coefficients measured on the Cu foil and on the Cu atoms implanted in Si_3N_4 are plotted together in Fig. 3(*a*). The similarity of the signals indicates that Cu atoms have mostly Cu neighbours in the Si_3N_4 matrix like in the Cu foil, and hence that Cu has precipitated during implantation instead of forming a compound with Si or N. The same result was found for Co implantation in Si_3N_4 (Zanghi *et al.*, 2001). Qualitatively, the fact that the oscillations have similar amplitudes suggests that Cu in the clusters has a coordination number similar to the bulk and, thus, precipitates have large diameters. A fit of good quality is obtained with phase and amplitude calculated for pure Cu (Fig. 3*b*). Quantitatively, the only detectable difference between the data extracted from the fits of the Cu bulk and the Cu clusters is a larger disorder for the clusters.

The oscillations extracted from the absorption coefficients measured on the three samples are displayed *versus* the temperature in Figs. 4, 5 and 6 for the Cu foil, the Co foil and the Cu clusters, respectively. The oscillation amplitudes are clearly damped when the temperature increases in the three cases.

The fit of our data is performed simultaneously on the whole data set, with the first, second and third cumulants as parameters. A structural disorder was also introduced together with a S_0^2 factor to account for inelastic losses. Since σ^2_{struc}, S_0^2 and the Debye temperature are not temperature-dependent, they were considered as global parameters, *i.e.* they affect the entire fit. Since σ^2 and C_3 are temperature-dependent, they were considered as free parameters for each set of data. The quality of the fits is illustrated in Figs. 3, 4 and 5, where they are plotted on the experimental oscillations. More detailed results will be given in a forthcoming paper. Extracted values from the fits are given in Table 1 for the Co foil and in Table 2 for the Cu foil and the Cu clusters. When possible, a comparison is made with values from the literature.

The S_0^2 factors given by the fits are in the usual range from 0.75 to 1 (Mustre de Leon *et al.*, 1991) for the three samples studied.

Values of the Debye temperature and of σ^2 at 300 K for bulk Co are presented in Table 1. The Debye temperature is found to be intermediate of those from the literature (Hou *et al.*, 2000; Ashcroft & Mermin, 1988; Kittel, 1966), and σ^2 is close to the value of Jacobs & Egry (1999) given for the Co–Co shell in the $Co_{80}Pd_{20}$ alloy. No C_3 parameter has to be introduced into the fit, indicating that the body distribution is normal.

Table 2
Debye temperature, $\Delta\sigma^2$ and ΔC_3 measured between 300 and 80 K, and S_0^2 deduced from the fit. An asterisk indicates that no error bar was given in the reference.

Sample	Θ_D (K)	$\Delta\sigma^2$ (10^{-3} Å^2)	ΔC_3 (10^{-4} Å^3)	S_0^2
Cu foil	305 (4)†	5.7 (3)†	2.2 (4)†	0.99 (2)†
	315 (*)‡	5.1 (2)§	1.3 (2)§	
	317 (5)§	6.0 (*)¶	1.6 (*)¶	
Cu clusters	285 (16)†	7 (1)†		0.99 (2)†

† Present work. ‡ Ashcroft & Mermin (1988). § Tröger *et al.* (1994). ¶ Bryan *et al.* (1997).

For bulk Cu, a third cumulant has to be introduced to obtain a fit of good quality in agreement with the work of Kiguchi *et al.* (2000) and Ashcroft & Mermin (1988), and its temperature dependence is quadratic as expected. Quantitative results (Table 2) such as the Debye temperature, $\Delta\sigma^2$ and ΔC_3 measured between 300 and 80 K are found to be close to values from the literature. The Debye temperature of bulk Cu is slightly smaller than those found by Ashcroft & Mermin (1988) and Tröger *et al.* (1994), the other values comparing well with previously calculated or measured ones (Tröger *et al.*, 1994; Bryan Edwards *et al.*, 1997). In addition, the Debye temperature for the Cu clusters is 7% smaller than the bulk temperature as expected for such systems.

The slopes of σ^2 *versus* T in the linear zone are different by a factor of 0.2 between bulk Cu and for the Cu clusters. This leads to a vibration frequency in the clusters that is smaller by a factor of 0.1 than in the Cu bulk.

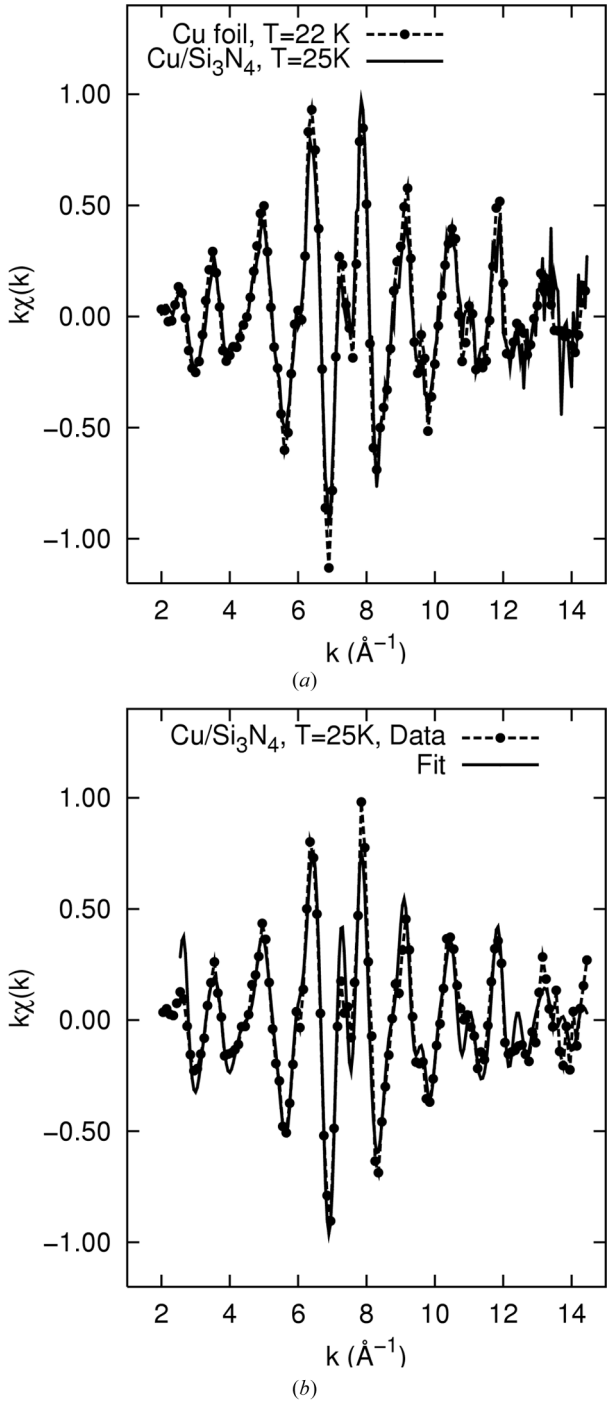

Figure 3
(*a*) Comparison between oscillations recorded on the Cu foil and on Cu implanted in Si_3N_4. (*b*) Fit of the oscillations recorded on Cu implanted in Si_3N_4.

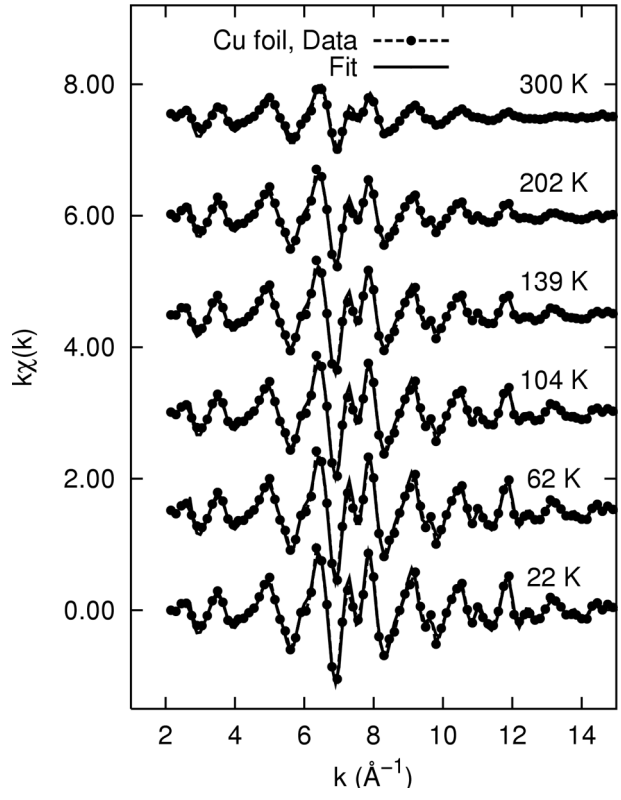

Figure 4
Oscillations extracted from the absorption coefficient measured on the Cu foil in transmission mode at different temperatures and their fit.

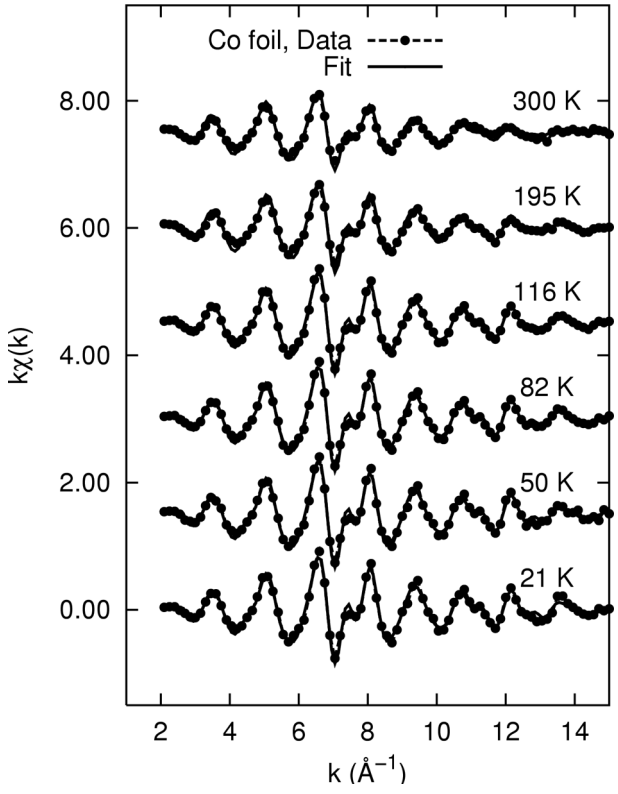

Figure 5
Oscillations extracted from the absorption coefficient measured on the Co foil in TEY at different temperatures and their fit.

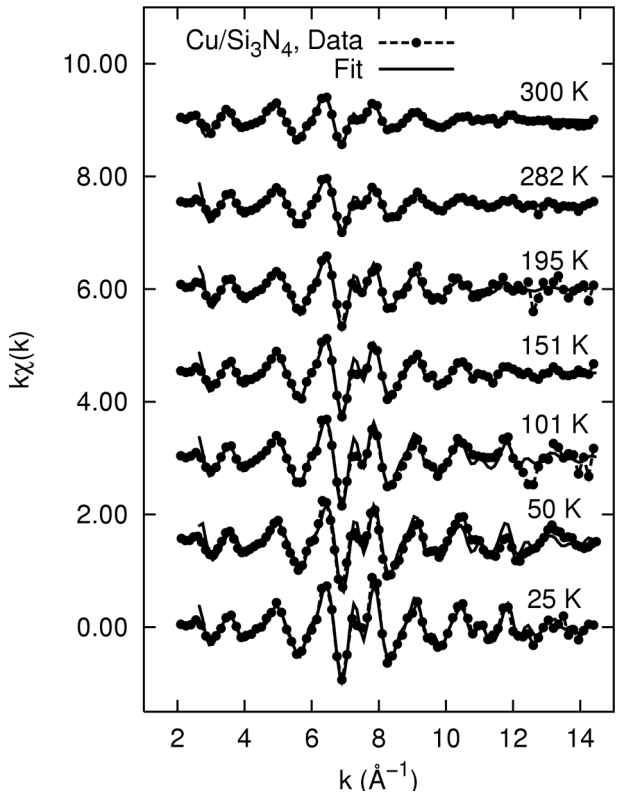

Figure 6
Oscillations extracted from the absorption coefficient measured on Cu clusters in TEY at different temperatures and their fit.

5. Conclusion

We have described a new device working between 4.2 and 300 K designed for the measurements of the absorption coefficients on a hard X-ray station of a synchrotron ring. When operating in the transmission mode, we checked by using a Cu foil that the temperature dependence of the absorption coefficient is the expected one. When operating in the TEY mode, values of the Debye temperature and of σ^2 for a Co foil are in agreement with those found in the literature. This indicates the good performance of the cryostat for temperature studies. Moreover, the low noise on the signal detected in TEY mode also insures measurements of good quality. The lower Debye temperature and vibration frequency measured in the Cu clusters are also proof that the device is operating well. The fluorescence detection mode was also checked without any difficulties.

This opens the field for new studies concerning vibration and thermal properties. The study of low-temperature phase transitions (Wang & Bunker, 1992) is another interesting application of this device, but it has not been tested yet.

To overcome problems with the sample thickness and/or low concentrations of the absorbing probe, TEY or fluorescence modes can be easily employed.

References

Andrieu, S., Fischer, H. M., Piécuch, M., Traverse, A. & Mimault, J. (1996). *Phys. Rev. B*, **54**, 2822–2829.

Ashcroft, N. W. & Mermin, N. D. (1988). *Solid State Physics.* Philadelphia, PA: Saunders.

Balerna, A. & Mobilio, S. (1986). *Phys. Rev. B*, **34**, 2293–2298.

Bohmer, W. & Rabe, P. (1979). *J. Phys. C*, **12**, 2465–2474.

Bryan Edwards, A., Tildesley, D. J. & Binsted, N. (1997). *Mol. Phys.* **91**, 357–369.

Chaumont, J., Lalu, F., Salomé, M. & Lamoize, A. M. (1981). *Nucl. Instrum. Methods*, **189**, 193–198.

Dalba, G. & Fornasini, P. (1997). *J. Synchrotron Rad.* **4**, 243–255.

Dalba, G., Fornasini, P., Gotter, R. & Rocca, F. (1995). *Phys. Rev. B*, **52**, 149–157.

Fornasini, P. (2001). *J. Phys. Condens. Matter*, **13**, 7859–7872.

Frenkel, A. I. & Rehr, J. J. (1993). *Phys. Rev. B*, **48**, 585–588.

Hou, M., El Azzaoui, M., Pattyn, H., Verheyden, J., Koops, G. & Zhang, G. (2000). *Phys. Rev. B*, **62**, 5117–5128.

Jacobs, G. & Egry, I. (1999). *Phys. Rev. B*, **59**, 3961–3968.

Kiguchi, M., Yokoyama, T., Matsumara, D., Kondoh, H., Endo, O. & Ohta, T. (2000). *Phys. Rev. B*, **61**, 14020–14027.

Kiguchi, M., Yokoyama, T., Terada, S., Sakano, M., Okamoto, Y., Ohta, T., Kitajima, Y. & Kuroda, H. (1997). *Phys. Rev. B*, **56**, 1561–1567.

Kittel, C. (1966). *Physique de l'Etat Solide.* Paris: Dunod.

Lee, J. M., Yoo, H. H. & Joo, M. (1999). *J. Synchrotron Rad.* **6**, 244–246.

Level, M. P., Brunelle, P., Chaput, R., Filhol, J. M., Herbeaux, C., Loulergue, A., Marcouillé, O., Marlats, J. L., Nadji, A., Tordeux, M. A., Chel, S. & Payet, J. (2002). *Proceedings of the 2002 European Particle Accelerator Conference*, 3–7 June 2002, Paris, France.

Michalowicz, A. (1991). *Logiciels pour la Chimie*, pp. 102–103. Paris: Société Française de Chimie.

Mimault, J., Faix, J. J., Girardeau, T., Jaouen, M. & Tourillon, G. (1994). *Meas. Sci. Technol.* **5**, 482–489.

Mustre de Leon, J., Rehr, J. J., Zabinski, S. I. & Albers, R. C. (1991). *Phys. Rev. B*, **44**, 4146–4156.

Newville, M. (2001). *J. Synchrotron Rad.* **8**, 96–100.

Pinto, A., Pennisi, A. R., Faraci, G., D'Agostino, G., Mobilio, S. & Boscherini, F. (1995). *Phys. Rev. B*, **51**, 5315–5321.

Proux, O., Mimault, J. & Girardeau, T. (2001). *Philos. Mag. A*, **81**, 2199–2215.

Roy, M., Gurman, S. J. & van Dorssen, G. (1997). *J. Phys. IV*, **7**(C2), 151–152.

Sevillano, E. & Meuth, H. (1979). *Phys. Rev. B*, **20**, 4908–4911.
Tourillon, G., Dartyge, E., Fontaine, A., Lemonnier, M. & Bartol, F. (1987). *Phys. Rev. A*, **121**, 251–257.
Tröger, L., Yokahama, T., Arvanitis, D., Lederer, T., Tischer, M. & Baberschke, K. (1994). *Phys. Rev. B*, **49**, 888–903.
Wang, Z. & Bunker, B. A. (1992). *Phys. Rev. B*, **46**, 11277–11283.
Zanghi, D., Traverse, A., Dallas, J.-P. & Snoeck, E. (2000). *Eur. Phys. J.* D**12**, 171–179.
Zanghi, D., Traverse, A., Gautrot, S. & Kaïtasov, O. (2001). *J. Mater. Res.* **16**, 512–523.
Zhang, K., Alexandrov, I. V., Valiev, R. Z. & Lu, K. (1998). *J. Appl. Phys.* **84**, 1924–1927.

 Received 16 December 2002 • Accepted 11 June 2003